Proceedings of the ASME 2010 3rd Joint US-European Fluids Engineering Summer Meeting and 8th International Conference on Nanochannels, Microchannels, and Minichannels
FEDSM-ICNMM2010
August 1-5, 2010, Montreal, Canada

FEDSM-ICNMM2010-30399

COMPRESSIBLE MICROCHANNEL FLOW

Gholamreza Mirshekari*
Mechanical Engineering Department
Université de Sherbrooke
Sherbrooke, QC, Canada, J1K 2R1
Email: g.mirshekari@usherbrooke.ca

Martin Brouillette
Mechanical Engineering Department
Université de Sherbrooke
Sherbrooke, QC, Canada, J1K 2R1

ABSTRACT

We present experiments on the isothermal gas flow at relatively high Mach numbers in microfabricated channels of small aspect ratios. The microchannels were fabricated by deep etching on silicon wafers, bonded to a Pyrex wafer to cover and seal them; the microchannels were 10 microns deep with a variety of widths. The accurate determination of the small flow rates was performed by measuring the displacement of a bead of mercury in a precision bore glass tube in a controlled environment. The experiment setup has been specially designed to account for inlet and outlet loss. The inferred friction coefficient at different values of Knudsen, Reynolds and Mach numbers shows that the flow inside the microchannel follows the classical laminar behavior over the range of experiments.

NOMENCLATURE

A Section area (μm^2)
a Width of microchannel (μm)
Bi Biot number
b Depth of microchannel (μm)
c_p Constant pressure specific heat (J/kg K)
D Diameter (μm)
f Coefficient of friction
h Convection heat transfer coefficient (W/m^{2}K)
Kn Knudsen number
k Thermal conductivity (W/m T)
L Length (μm, mm)
M Mach number
$\dot{m}$ Mass flow rate (kg/s)
P Pressure (Pa)
$\dot{Q}$ Heat transfer rate (W)
T Temperature (°C)
u Velocity (m/s)
y Direction normal to the surface
γ Specific heats ratio
Δ Friction loss (N)
θ The temperature difference between solid and ambient (°C)
Λ Mean free path (Å)
μ Viscosity (Ns/m^2)
ρ Density (kg/m^3)
τ Wall thickness (mm)
ω Tangential momentum accommodation coefficient

1 Introduction

The newly arrived science of microfluidics has raised increasing questions about the different aspects of micro-flows in the vast variety of new applications in the bioengineering, microelectromechanical system, energy harvesting, etc. thanks to the intense research efforts, accomplished in the past decades many of the unusual characteristics of the flow at micro and nano-scale are now clarified. It is now well known that due to the increased "surface to volume ratio" of fluidic systems at microscale, the transport phenomena become dominant in such flows.

Microchannels as the elementary components used in the microfluidics devices have attracted more attention. The flow

*Address all correspondence to this author.

in microchannels has been the the subject of many experimental, numerical and analytical research projects [1] [2] [3] [4] [5]. These researches cover a variety of flow regimes form rarefied to hydrodynamic. Gad el Hak [1] provided a methodical approach to the flow modelling for a broad variety of micro-devices. He presented a survey of broad available methodologies to model and compute transport phenomena within the micro-devices. Roy et al. [6] developed a two-dimensional finite element-based microscale flow model to efficiently predict the overall flow characteristics up to the transition regime for reasonably high Knudsen number[1] flow inside the microchannels and nano-pores. Their presented two-dimensional numerical results for Poiseuille flow of a simple fluid through the microchannel were comparable to the numerical and experimental data. Hajiconstantinou and Simek [7] investigated the constant-wall-temperature convective heat-transfer characteristics of fully developed two-dimensional flow in micro and nano-channels. Their investigation covers the slip flow and transition regimes using slip-flow theory in the presence of axial heat conduction. Their results show that the slip-flow prediction is in good agreement with the Direct Simulation of Monte Carlo results for $Kn < 0.1$, and that the Nusselt number decreases monotonically with increasing Knudsen number in the fully accommodating case, both in the slip flow and transition regimes. Jain and Lin [8] performed numerical simulation of nitrogen gas flow in the long square cross-section microchannels. They used a three-dimensional continuum model with slip and no-slip boundary conditions at room temperature and atmospheric outlet pressure and validated the results with the available experimental and numerical results. They have found that for incompressible flow when D_h is less than 60 μm, a slip boundary condition must be applied. For compressible flow, a parametric study was conducted for $D_h = 1\mu$m and $L/D_h = 200$ and variable pressure ratios that turns out that the increase in pressure ratio leads to increase in compressibility effects while the rarefaction effects start diminishing. Renksizbulut et al. [9] numerically investigated the rarefied gas flow and heat transfer in the entrance region of rectangular microchannels in the slip-flow regime. They examined the effects of Reynolds number, channel aspect ratio, and Knudsen number on the simultaneously developing velocity and temperature fields. They observed very large reductions in the entrance region, the friction factor and Nusselt number due to the rarefaction effects. Ewart et al. [2] measured the helium mass flow rate in a wide range of Knudsen number from hydrodynamic to near free molecular and compared with the theoretical first-order slip continuum approach and theoretical values calculated from kinetic approaches. Arkilic et al. [3] reported the experiment aimed at measuring Tangential Momentum Accommodation Coefficient (TMAC) for several gases in silicon microchannels. For all investigated gases the TMAC is found to be lower than one, ranging from 0.75 to 0.85. The recent experiments by Pitakarnnop et al [10] show that the TMAC is very close to unity. Harley et al. [11] experimentally and theoretically investigated the low Reynolds number, high Mach number subsonic flow in microchannels. Their measured friction factor was in good agreement with the theoretical prediction for isothermal first-order slip flow. Chong [12] studied the choked gas flow in microchannels using the method of Direct Simulation Monte Carlo (DSMC). He observed that for a microchannel the choking happens only at the exit. He also compared the DSMC results with the Navier-Stokes isothermal solution and concluded that the mass flux can be estimated by Navier-Stokes relations if the microchannel is enough long.

The above mentioned literature studied the subsonic compressible flow in a variety of regimes. In fact, in the steady frictional flow inside the constant area microchannels the flow chokes and the supersonic flow are impossible. In addition in most of experiments on the flow in microchannels the measured pressure across the channel is the pressures inside large reservoirs connected to the inlet and outlet of the channel. These are actually the total pressures of flow at the entrance and the outlet of channel assuming the friction in the inlet and the outlet ports are negligible. This is, of course, a reasonable assumption for low Mach number flows. However, since the friction in the inlet and outlet ports are proportional to the square of flow velocity, this can not be a good assumption at higher values of Mach number. Therefore, in this experiment we also proceed to evaluate and remove the effects of friction in the inlet and the outlet of the microchannels. The experiments would be established in the relatively high pressures and increased values of Reynolds number and we try to impose the isothermal condition in the experiment.

2 Theory

2.1 General comments on duct flow

Assuming one-dimensional adiabatic steady viscous flow of a perfect gas with constant specific heats through a constant area channel, the energy and continuity equations can be integrated along the channel to obtain the Fanno line flow. Practically, however, it is necessary to determine the change of properties with actual duct length and this requires the use of the momentum equation, with a term accounting for friction forces acting on the control volume. The details of such a calculation can be found in Thompson [13] and the resulting relation is:

$$\frac{fL_{max}}{D_h} = \int_M^1 \frac{2\left(1-M^2\right)\dfrac{dM}{M}}{\left(1+\dfrac{\gamma-1}{2}M^2\right)\gamma M^2} \tag{1}$$

In this equation f is the coefficient of friction which is related to the Reynolds number and roughness of the channel, L_{max} is

[1] The Knudsen number (Kn) is defined as the ratio of mean free path of the molecules to the characteristic dimension of the flow

the length needed for the flow with certain Mach number at the entrance (M_1) to become choked at the exit ($M_2 = 1$) and D_h is the hydraulic diameter [2] of the channel.

In the gas flow inside the micro channel, the gas could be in thermal equilibrium with the surrounding solid walls. This flow has different characteristics from Fanno flow, involving heat transfer as well as friction. For such a flow, integrating the continuity, momentum and energy equations results in

$$\frac{fl}{D_h} = \frac{1}{\gamma {M_1}^2} - \frac{1}{\gamma {M_2}^2} + \ln \frac{{M_1}^2}{{M_2}^2} \tag{2}$$

and also because the fluid goes through an isothermal process

$$\frac{M_1}{M_2} = \frac{P_2}{P_1} = \frac{\rho_2}{\rho_1}\ . \tag{3}$$

Unlike the Fanno flow, the critical Mach number in isothermal flow is not 1, but $M = 1/\sqrt{\gamma}$. This means that for $M < 1/\sqrt{\gamma}$, M increases along the channel, whereas for $M > 1/\sqrt{\gamma}$, M decreases. Assuming laminar flow, the coefficient of friction (f) in the channel is $64/Re$ [14]. For the uniform cross section channel the Reynolds number along the channel is constant

$$Re = \frac{\rho_1 u_1 D_h}{\mu} = \frac{\dot{m}}{\mu (A/D_h)} \tag{4}$$

where $\dot{m}$ is the mass flow rate and A is the cross section area of the channel. For sonic flow of atmospheric air in a 10 μm hydraulic diameter and 1 mm long microchannel, which is our desired geometry of the experiment, $f \approx 0.3$ and therefore

$$\frac{fl}{D_h} = \frac{64l}{ReD_h} = \frac{0.3 \times 1000\mu\text{m}}{10\mu\text{m}} = 30 \tag{5}$$

and the scaling parameter[3] is $ReD_h/4L = 0.533$. To have a better understanding of the behavior of the flow in such a channel, assume that the air enters the channel with Mach number M_1 and chokes at exit. Equations 2 and equation 3 can be combined to obtain

$$\frac{64L}{ReD_h} = \frac{1}{\gamma {M_1}^2}\left[1 - \frac{1}{\left(\frac{P_1}{P_2}\right)^2}\right] - 2\ln\frac{P_1}{P_2} \tag{6}$$

[2]For a rectangular section channel the hydraulic diameter is $D_h = 2ab/a+b$ where a and b are width and height of channel respectively.

[3]The scaling parameter introduced by Brouillette [15] to quantify the effect of scale in the compressible micro-flows is defined as $ReD_h/4L$

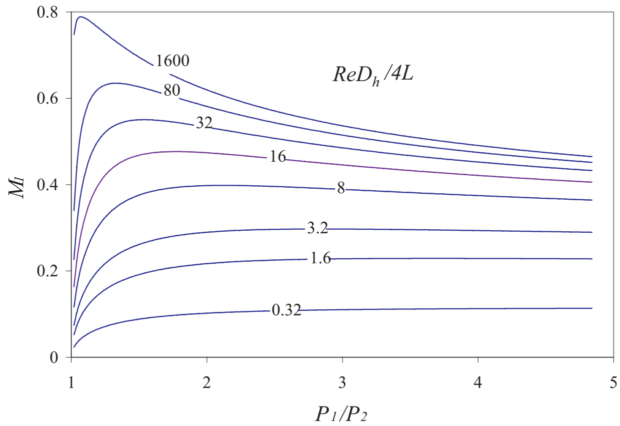

FIGURE 1. Plot of entrance Mach number versus pressure ratio across the channel for different values of scaling parameter($\gamma = 1.4$)

Figure 2.1 represents the variation of M_1 versus pressure ratio at different values of scaling parameter. It can be seen from this figure that, for a certain channel, the Mach number cannot be increased considerably by increasing the pressure ratio across the channel. To achieve higher Mach numbers, the value of scaling parameter should be greater. For a fixed geometry this can be obtained by increasing P_1. For example, it can be seen from the figure that an entrance pressure of 100 atm (scaling parameter equal to 32) can produce Mach number about 0.55 for pressure ratio of 1.5. Practically, it is not easy to obtain the steady transonic flow of gas in the microchannels. The Mach number along the channel increases and in the limit it reaches to the value of $1/\sqrt{\gamma}$.

2.2 Microchannel flow at rarefied regimes

In the previous discussion the flow in the microchannel is assumed to be within the continuum approximation. However, the rarefaction effects could be important for some microchannel flows. Usually, to evaluate the effects of rarefaction in flow we refer to the Knudsen number of flow. For a sufficiently rarefied macro-scale flow or a moderate pressure microscale flow the value of Knudsen number can be large enough such that the fluid cannot be considered as a continuum and thus we must consider the interaction between the individual molecules and the surfaces. Using the kinetic theory of gases, the Knudsen number can be expressed in terms of the Mach number and the Reynolds number [1]

$$Kn = \frac{3}{2}\sqrt{\frac{\pi\gamma}{2}}\frac{M}{Re}\ . \tag{7}$$

It can be seen that the rarefied gas flow can occur at a combination of high Mach numbers and low Reynolds numbers. In our

TABLE 1. The analogy between boundary conditions for laminar flow of gas in a microchannel and heat dissipation in a solid ($\theta = T - T_a$).

Conduction in a solid rod	Microchannel flow
$\theta = 0$	$u = 0$ (No slip)
$\frac{\partial \theta}{\partial n}\|_w = \frac{\dot{q}_w}{k_s}$ (or 0)	$\frac{\partial u}{\partial n}\|_w = \frac{\tau_w}{\mu}$ (or 0)
$\frac{\partial \theta}{\partial n}\|_w = \frac{h}{k_s}\theta\|_w$	$\frac{\partial u}{\partial n}\|_w = \frac{1}{\Lambda}\frac{\omega}{2-\omega}u\|_w$ (1st order slip)

desired experiment on the microchannel flow, the pressure may vary between 100 kPa and 10 MPa. The Knudsen number thus varies between 10^{-2} and 10^{-4}. This flow is a continuum flow which can be assumed as slip flow in low pressures and as no-slip flow in higher pressures.

In the no-slip condition the velocity near the wall is very small and the flow field can be determined with respect to this boundary condition. In the slip flow, since the scale commensurate with the mean free path of the gas, the velocity at the wall is no longer considered small. In this case, the velocity near the wall is commonly described by the Maxwellian boundary condition

$$\left.\frac{\partial u}{\partial y}\right|_{y=0} = \frac{1}{\Lambda}\frac{\omega}{2-\omega}\, u|_{y=0} \tag{8}$$

where ω is the Tangential Momentum Accommodation Coefficient (TMAC) which can vary from 0 for a completely specular momentum accommodation to 1 for a completely diffusive momentum accommodation.

Interestingly, the slip boundary condition in a microchannel flow is analogous to the convective heat transfer boundary condition for the conduction in a solid rectangular long rod as mentioned in Table 1. In this context the Knudsen number could be analogous to the inverse of Biot number which is defined as the ratio of the internal thermal resistance of a solid to the boundary thermal resistance ($Bi = hD/k_s$).

3 Experiment

The experiment was planned to measure the pressure difference and the flow rate across the microchannels. For the design of the experiment setup it was necessary to estimate the measurands. Table 2 shows the values of pressure for the tests. The maximum pressure in the tests is not more than 20 bars to ensure that deviation from ideal gas is less than 1% [16]. The minimum pressure in the tests is the atmospheric pressure, therefore, there is no need for evacuation. The experiment setup should

TABLE 2. The values of pressure at the entrance and exit of microchannel in the experiments

	Test I	Test II	Test III	Test IV
P_{t1} (kPa)	310	550	965	1725
P_{t2} (kPa)	101-275	101-495	101-860	101-1550

allow us to provide and measure the pressures around 10 MPa. A schematic diagram of experiment setup is shown in Fig. 2. It consists of a chamber to install the microchannels and establish the inlet and outlet connections. The measurement of flow rate is performed by means of the movement of a mercury bead inside a precision bore glass tube. This setup was entirely immersed in an ice-water tank to ensure a uniform and constant temperature environment needed for the flow measurement. The total pressures P_{t1} and P_{t2} across the microchannel are measured with 2.5% error. For the choked microchannel, the minimum and maximum of P_{t1} are 320 kPa and 2 MPa respectively and the minimum and maximum of P_{t2} are 100 kPa and 1.7 MPa.

The microchannels were fabricated by anodic bonding of silicon wafer and a pyrex wafer as shown in figure 2. The channel and plenums were etched on the silicon substrate. Then the substrate etched to the back to create the inlet and outlet holes. These microfabrication procedure is simple but not perfect method to build the microchannels. There is about 0.1 μm tolerance in the dimensions and the surfaces are not perfectly smooth except for the covering Pyrex slab where the roughness is something less than 5 nm. For the etched trenches in the silicon substrate the sidewalls have scallops of about 50 nm which caused by the cycling nature of the Deep Reactive Ion Etching (DRIE). However, these scallops are perpendicular to the direction of the flow and they should not have remarkable effect on the flow. For the bottom of the channels the micro-masking effect results in grass like surface texture with a roughness up to 50 nm. Recently these imperfections can be overcome by using improved etch recipes and the use of Silicon On Insulator (SOI) technology.

In order to study the effects of geometry on the flow, the tests have been established in a few geometrically different microchannels by measuring the flow rate ($\dot{m}$) at different values of P_{t1} and P_{t2}.

3.1 Gas flow measurement

The estimated volumetric flow rate in the microchannel at the Mach number of 0.55 in the entrance is equal to 1.133 ml/min. Such a small flow rate of gas cannot be measured easily by ordinary commercial flowmeters. This flow rate could be measured by a method based on the accumulation of gas and measuring the increase in either pressure or the volume of the gas. For a perfect gas, in an isothermal constant volume measure-

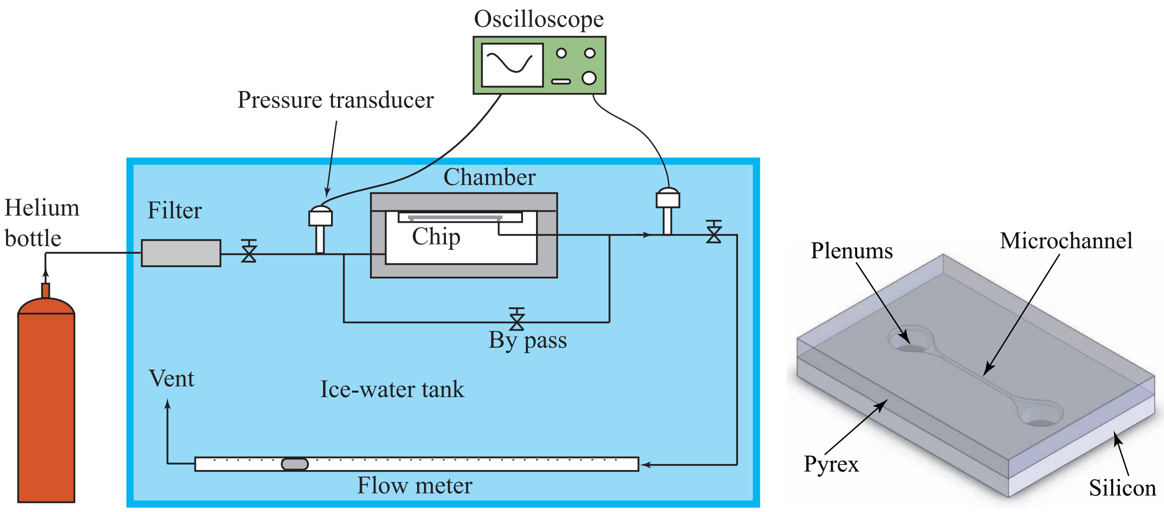

FIGURE 2. Schematic of experiment setup and the microchannel

ment system, the accumulation of mass results in the increase of pressure and in a constant pressure system the accumulation of mass results in the increase of the volume of the accumulated gas. For better accuracy in our experiment a constant pressure system produces more accurate results. In both approaches the overall mass of the gas in the system is an important parameter that reduces the measurement errors. A precision bore glass tube (2.999 ± 0.005 mm ID $\times$ 1016 mm length) was used as a cylinder an a bead of mercury as a piston. The constant temperature is provided by an ice-water two phase medium. The melting temperature of ice has a negligible dependence on the pressure. Based on the meteorological data from Environment Canada, the atmospheric pressure in Sherbrooke can have a maximum variation of ± 2 kpa during a day and of course it has a smaller variation during a test time which is about an hour. The error in reading the distance passed by the mercury bead is about 1 mm or 0.1% of tube length. For the previously mentioned tube, the total error in measuring the volume is about 0.43% and the distance travelled by mercury bead, respectively, and the overall error in measuring the mass is around 1.43%.

3.2 Refinement of experimental data

To calculate the Mach number and static pressures at the entrance and the outlet of the channel, we refer to the control volume shown in the figure 3. The process from condition $t1$ to the condition 1 is assumed to be isothermal. The conservation laws along with the equation of state for an isothermal process

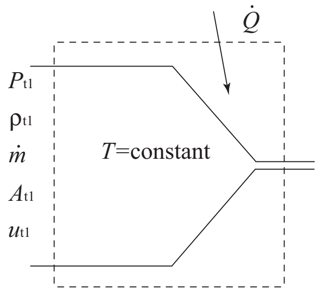

FIGURE 3. The control volume surrounding the inlet or outlet port used to calculate the thermodynamical properties at entrance and exit of channel

for this control volume are

$$\begin{aligned}
&\rho_{t1} u_{t1} A_{t1} = \rho_1 u_1 A_1 = \dot{m} \\
&P_{t1} A_{t1} + \dot{m} u_{t1} = P_1 A_1 + \dot{m} u_1 \\
&\dot{m}\left(c_p T + \frac{{u_{t1}}^2}{2}\right) + \dot{Q} = \dot{m}\left(c_p T + \frac{{u_1}^2}{2}\right) \\
&\frac{P_{t1}}{P_1} = \frac{\rho_{t1}}{\rho_1}
\end{aligned} \tag{9}$$

Since the pressure transducers are connected to the large scale inlet and outlet ports that have diameter about 10^3 times greater than the diameter of microchannels (10^6 times greater section area), u_{t1} in momentum and energy equations can be neglected and also it can be assumed that the measured pressures

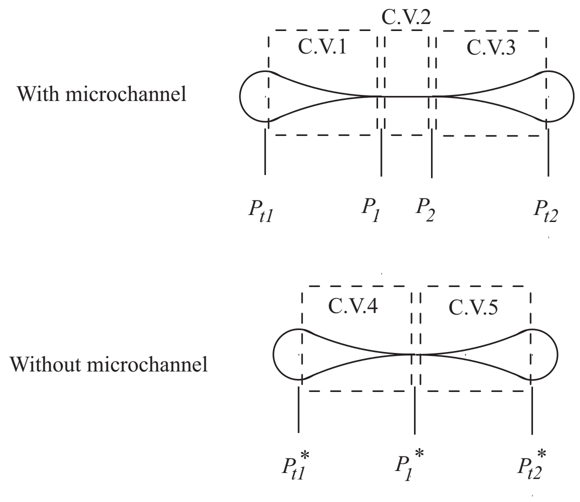

FIGURE 4. The Control volumes (C.V.) used to quantify the plenum losses

are the total pressures of gas. After simplification, the two unknown values P_1 and u_1 can be calculated form this simultaneous system of equations

$$\begin{cases} P_{t1}A_{t1} - P_1 \alpha {D_h}^2 = \dot{m}u_1 \\ P_1 = \dfrac{\dot{m}P_{t1}}{\rho_{t1}\alpha {D_h}^2 u_1} \end{cases} \tag{10}$$

this procedure can be followed to calculate both the entrance and the exit properties. The Reynolds number can be calculated from Eq. 4.

In order to quantify the effects of inlet and outlet plenums on the chip, a chip that has only the inlet and outlet plenums with zero channel length goes through a set of carefully controlled tests. The following calculation with respect to the notation in Fig. 4 has been done: For the flow through the microchannels, the conservation of momentum equation for three control volumes surrounding the inlet plenum, the channel, and the outlet plenum can be written as:

$$\begin{array}{ll} \text{C.V.1}: & P_{t1}A_{t1} + \dot{m}V_{t1} = P_1A_1 + \dot{m}V_1 + \Delta_1 \\ \text{C.V.2}: & P_1A_1 + \dot{m}V_1 = P_2A_1 + \dot{m}V_2 + \Delta_{1-2} \\ \text{C.V.3}: & P_2A_2 + \dot{m}V_2 = P_{t2}A_{t2} + \dot{m}V_{t2} + \Delta_2 \end{array} \tag{11}$$

where Δ_1, Δ_{1-2} and Δ_2 are the friction losses in the inlet plenum, the channel, and the outlet plenum respectively. The same equations can be written for the chip without channel.

$$\begin{array}{ll} \text{C.V.4}: & P_{t1}^*A_{t1} + \dot{m}V_{t1}^* = P_1^*A_1 + \dot{m}V_1^* + \Delta_1^* \\ \text{C.V.5}: & P_1^*A_1 + \dot{m}V_1^* = P_{t2}^*A_{t2} + \dot{m}V_{t2}^* + \Delta_2^* \end{array} \tag{12}$$

where the superscript $*$ denotes the values for the chip without channels. From the test on the chip without channel

$$\Delta_1^* + \Delta_2^* = P_{t1}^*A_{t1} + \dot{m}V_{t1}^* - P_{t2}^*A_{t2} + \dot{m}V_{t2}^* = \text{known}. \tag{13}$$

To obtain the values of Δ_1^* and Δ_2^* separately, the ratio of Δ_1^*/Δ_2^* should be determined. The geometry of inlet and outlet plenums are the same but the direction of flow in them are opposite. However, since the hydraulic diameter along the plenums does not have a large variation, the number of unknowns can be reduced assuming that

$$\left.\begin{array}{l} \Delta_1^* \propto [\rho_{t1}A_{t1}V_{t1}^2]^* \\ \Delta_2^* \propto [\rho_{t2}A_{t2}V_{t2}^2]^* \end{array}\right\} \Rightarrow \frac{\Delta_1^*}{\Delta_2^*} = \frac{\dot{m}V_{t1}^*}{\dot{m}V_{t2}^*} = \frac{V_{t1}^*}{V_{t2}^*} = \frac{P_{t2}^*}{P_{t1}^*} \tag{14}$$

and calculate the values of Δ_1^* and Δ_2^*. Now, the values of Δ_1 and Δ_2 can be determined by performing the tests on the chip that has no microchannel. The flow rate and pressure in these tests were carefully controlled to generate data necessary for the following argument

In the tests at same $\dot{m}$ and P_{t1}: $\Delta_1 = \Delta_1^*$
In the tests at same $\dot{m}$ and P_{t2}: $\Delta_2 = \Delta_2^*$

The calculated values of Δ_1 and Δ_2 were then subtracted from the pressure drops across the chips leaving the net pressure differences across the microchannels.

4 Results and discussion

Figure 5 shows the examples of the raw experimental data. The two microchannels (I and II) in each drawing are fabricated to have the same geometry. The microchannel in the bottom drawing is 10 times longer than that in the top drawing. The differences between two series of results in each diagram originate from the obvious differences in inlet total pressures as well as possible small differences in dimensions resulting from microfabrication inaccuracy. The graphes show the expected behavior of increasing flow rate as a function of decreasing the outlet pressure. The choking of microchannels are also seen in the graphes. Obviously the values of the flow rate in the longer microchannel is less than the shorter microchannel, however, since in these graphes the effect of inlet and outlet plenums are not eliminated, the quantitative comparison may not be credible.

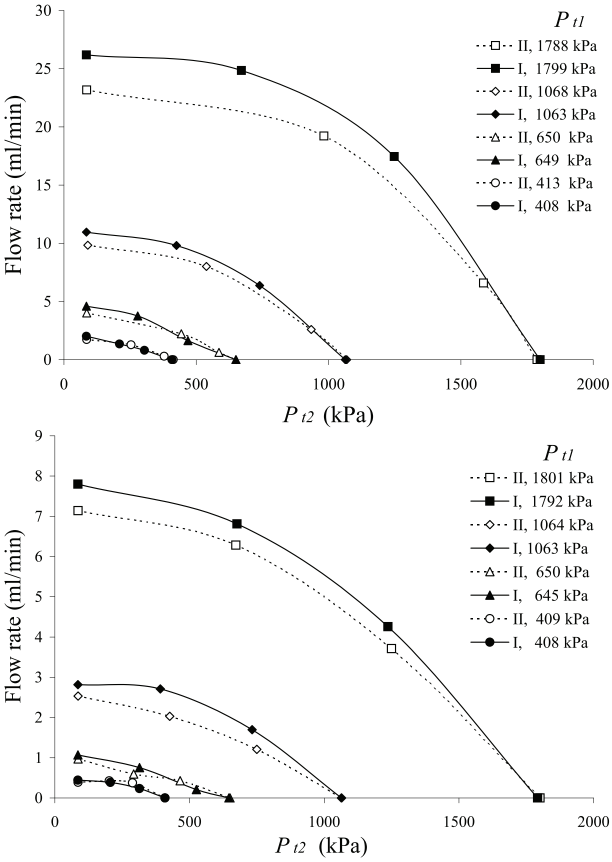

FIGURE 5. Volumetric flow rate as a function of total outlet pressure at different values of total inlet pressure (raw data). The two microchannels in the top figure are $300 \pm 1\mu$m long, $12.10 \pm 0.1\mu$m wide and $10.05 \pm 0.1\mu$m deep. The two microchannels in the bottom figure are $3000 \pm 1\mu$m long, $13.24 \pm 0.1\mu$m wide and $9.55 \pm .01\mu$m deep.

To observe the effect of geometry (i.e., L/D_h) on the flow, geometrically different microchannels have been fabricated and tested. Figure 6 represents the variation of inlet Mach number (M_1) as a function of normalized pressure difference across the microchannels. The pressures in this graph are static pressures calculated as explained in section 3.2. These four different geometries were tested at inlet pressure of $P_{t1} = 1800$ kPa. In Fig. 6 the flow has the similar behavior for different geometries which is increase in inlet Mach number until the microchannel chokes. As expected in section 2.1, it is the tightness of the microchannel (L/D_h) who determines the final value of inlet Mach number.

Figure 7 shows the values of entrance Mach number versus scaling parameter at different pressure ratios. The experimentally measured values are compared with the theoretical values of the isothermal flow from equation 6. No significant difference can be seen between the two categories of data and this upholds the

L/D_h	$a(\mu\mathrm{m})$	$b(\mu\mathrm{m})$	$L(\mu\mathrm{m})$
27.32	12.1	10.05	300
79.49	5.50	10.18	571
96.52	27.62	9.95	1412
270.36	13.24	9.55	3000

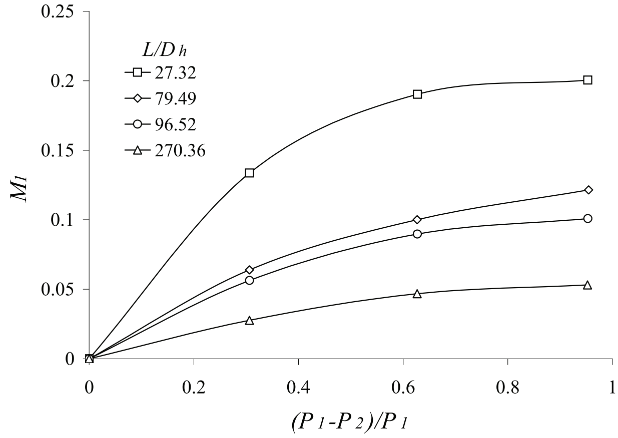

FIGURE 6. The measured entrance Mach number as a function of normalized pressure difference for different microchannels

validity of isothermal assumption for the steady flow of gas in microchannels etched in silicon substrates.

The validity of isothermal flow assumption in the experiment can be verified assuming a control volume surrounding the chamber shown in Fig. 2. The amount of overall heat absorption during the isothermal expansion of air from, for example, 10 MPa in the inlet port to 2 bar at the outlet port. The corresponding flow rate for this condition is about 50 mg/min and the heat absorption is

$$\dot{Q} = \dot{m}\left(\frac{{u_2}^2}{2} - \frac{{u_1}^2}{2}\right) = 1.004 \times 10^{-6}\mathrm{W} \;\; (T_1 = T_2) \tag{15}$$

The chamber can be modeled as a cylindrical piece of stainless steel with the microchannel located in the middle of it sunk in the ice water mixture at 0 °C. The temperature difference across the chamber walls at which the above calculated heat absorbtion takes place, is

$$\Delta T \approx \frac{\dot{Q}\tau_{wall}}{k_{steel}A_{wall}} = 4.96 \times 10^{-8}\mathrm{K} \tag{16}$$

where τ_{wall} is the chamber's wall thickness and A is the chamber's overall surface. This calculated temperature difference is certainly negligible in this experiment.

The more detail on heat transfers in the inlet and the outlet ports of channel can be calculated by correlation recommended by Whitaker appeared in Incropera De Witt [17] for the flow of fluid inside a channel at constant wall temperature. The calculated convection heat transfer coefficient (h) is equal to $12755\mathrm{W/m^2K}$. The amount of heat transfer in the isothermal acceleration of 60 mg/min air to the Mach number of 0.55 is roughly 2×10^{-2}W. Using the above convective heat transfer coefficient, the temperature difference needed to dissipate this heat transfer in a 1 mm^2 surface is about 1.57 K which is not a large temperature difference. In fact, this calculation is done for highest predicted Reynolds number and for the lower Reynolds numbers the temperature difference would be smaller since the Nusselt number is proportional to $\sqrt[3]{Re}$ while the flow rate is proportional to Reynolds number. As a conclusion, the flow in the microchannel, itself, can be assumed to be completely isothermal and the assumption of isothermal flow for the inlet and outlet plenums produces an error around 1%.

The small discrepancies between two types of data is seen at lower pressure ratios and higher scaling parameters. This is not surprising since the higher scaling parameter means lower momentum and thermal diffusion which cause the flow to start to differ from isothermal flow and this consequently results in higher Mach number.

The measured friction coefficient versus Reynolds number at different values of Knudsen number is shown in Fig. 8. It clearly shows that the flow inside the microchannel follows, almost, the laminar behavior over the experiment's range of Knudsen numbers. However, for higher values of Knudsen number, the flow starts to differ from the laminar behavior. This is, of course, the transition from no-slip flow to slip flow that takes place at Knudsen numbers around 0.007. According to Gad el Hak [1], the no-slip and no temperature jump boundary condition should be assumed for flow with Knudsen number less than 0.001 and the first order slip and temperature jump should be assumed for $0.001 < Kn < 0.1$. Therefore, based on his criteria, all of these experiment results lay in the realm of continuum flow with slip and temperature jump boundary conditions. Since the velocity near the wall for a slip flow is no longer equal to zero, the shear stresses in boundary layer are less compared to those of the no-slip flow and that explains the smaller values of friction factor for the slip flow regime.

The scattered data in Fig. 8 are possibly caused by the different aspect ratio of the microchannels. The friction factor (f) is usually defined for a tube. In addition the microfabrication inaccuracy specially in inlet and outlet plenums can produce errors in data. The wrong choice of geometry for the plenums and the defected plenums are the major reasons for the scattered data.

4.1 Conclusion

The steady flow of compressible gas in microchannels with different hydraulic diameters, Reynolds numbers and Mach numbers has been experimentally studied. From this study it has been revealed that rarefaction effects start to appear from Knudsen number greater than 0.007 and the flow in the experiment's range can be fairly explained by laminar no-slip assumption. The experimental results confirm the assumption of isothermal flow in microchannels.

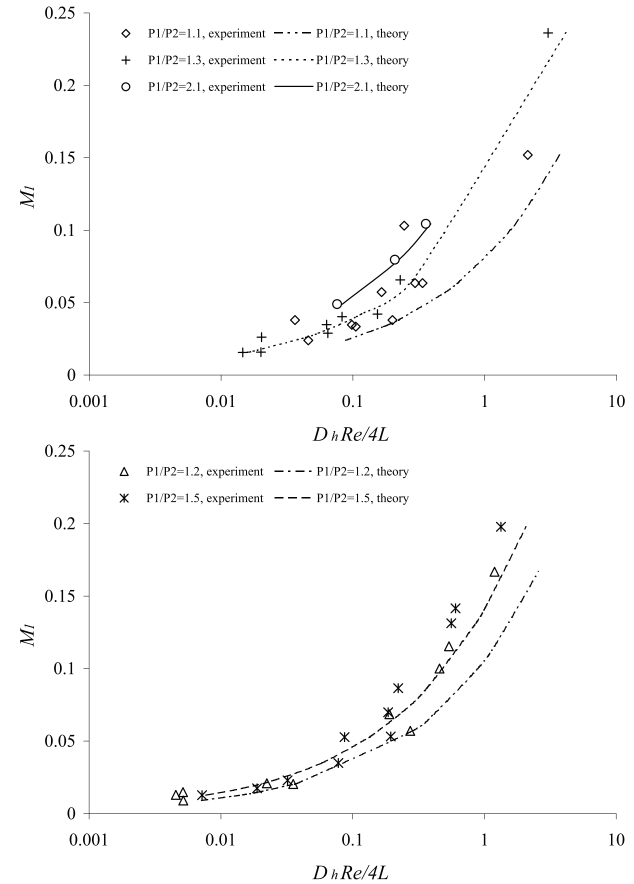

FIGURE 7. Comparison of measured and calculated (Equation 6) entrance Mach number versus scaling parameter at different pressure ratios

ACKNOWLEDGMENT

This work is supported by the Natural Sciences and Engineering Research Council (NSERC) of Canada. Also, the first author acknowledges the Iranian Ministry of Science, Research and Technology (MSRT) for the scholarship awarded.

The authors would like to thank professor Luc G. Frechette in mechanical engineering department of university of Sherbrooke for his advice and many helpful conversations in different topics related to this project.

REFERENCES

[1] Gad el Hak, M., 2001. "Flow physics in mems". *Mechanics and Industries,* **2**(44), pp. 313–341.

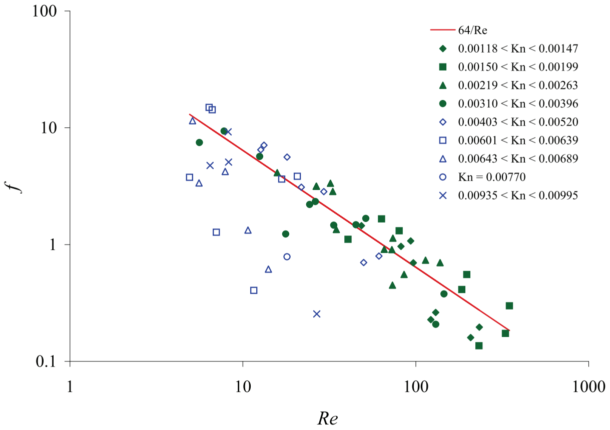

FIGURE 8. The measured friction coefficient as a function of Reynolds number for different ranges of Knudsen numbers.

[2] Ewart, T., Perrier, P., Graur, I., and Molans, J. G., 2007. "Mass flow rate measurements in a microchannel, from hydrodynamic to near free molecular regimes". *Journal of Fluid Mechanics,* ***584***, pp. 337–356.

[3] Arkilic, E. B., Breuer, K. S., and Schmidt, M. A., 2001. "Mass flow and tangentional momentum accommodation in silicon micromachined channels". *Journal of Fluid Mechanics,* ***437***, pp. 29–43.

[4] Zohar, Y., Lee, S. Y. K., Lee, W. Y., Jiang, L., and Tong, P., 2002. "Subsonic gas flow in a straight and uniform microchannel". *Journal of Fluid Mechanics,* ***472***, pp. 125–151.

[5] Morini, G. L., Lorenzini, M., and Salvigni, S., 2006. "Friction characteristics of compressible gas flows in microtubes". *Experimental Thermal and Fluid Science,* ***30***, pp. 733–744.

[6] Roy, S., Raju, R., helen F. Chuang, Cruden, B. A., and Meyyappan, M., 2003. "Modeling gas flow through microchannels and nanopores". *Journal of Applied Physics,* ***93***(8), pp. 4870–4879.

[7] Hajiconstantinou, N. G., and Simek, O., 2002. "Constant-wall-temperature nusselt number in micro and nanochannels". *ASME Journal of Heat transfer,* ***124***, pp. 356–364.

[8] Jain, V., and Lin, C. X., 2006. "Numerical modeling of three-dimensional compressible gas flow in microchannels". *Journal of micromechanics and microengineering,* ***16***, pp. 292–302.

[9] Renksizbulut, M., Niazmand, H., and Tercan, G., 2006. "Slip-flow and heat transfer in rectangular microchannels with constant wall temperature". *International Journal of Thermal Sciences,* ***45***, pp. 870–881.

[10] Pitakarnnop, J., Varoutis, S., Valougeorgis, D., Geoffroy, S., Baldas, L., and Colin, S., 2010. "A novel experimental setup for gas microflows". *Microfluid Nanofluid,* ***8***(1), pp. 57–72.

[11] Harley, J. C., Huang, Y., and Z, H. H. B. J. N., 1995. "Gas flow in micro-channels". *Journal of Fluid mechanics,* ***284***, pp. 257–274.

[12] Chong, X., 2006. "Subsonic choked flow in the microchannel". *Physics of Fluids,* ***18***, pp. 127104–127108.

[13] Thompson, P. A., 1972. *Compressible-fluid dynamics*. McGraw Hill.

[14] White, F. M., 2003. *Fluid Mechanics*. McGraw-Hill.

[15] Brouillette, M., 2003. "Shock waves at microscales". *Shock waves,* ***13***, pp. 3–12.

[16] Stroud, L., Miller, J. E., and Brandt, L. W., 1960. "Compressibility of helium at -10 to 130 f and pressures to 4000 psia". *Journal of Chemical and engineering Data,* ***5***(1), p. 51.

[17] Incropera, F. P., and Witt, D. P., 2002. *Fundamentals of Heat and Mass Transfer*. Wiley.